INORGANIC CHEMISTRY
FRONTIERS

RESEARCH ARTICLE

View Article Online
View Journal | View Issue

Cite this: *Inorg. Chem. Front.*, 2025, **12**, 8000

Chiral molecular 4f qubits by post functionalization

Steen H. Hansen,*[a] Christian D. Buch, [a] Bela E. Bode *[b] and Stergios Piligkos *[a]

We herein demonstrate the synthesis of a pair of enantiomerically pure Yb^{III} complexes by post-functionalisation of the parent Yb^{III} complex *via* condensation with an enantiomerically pure chiral amine. The enantiomeric pair is structurally characterised by single crystal and powder X-ray diffraction, showing that it crystalises in the $P2_12_12_1$ Sohncke space group with Flack parameters close to zero, which confirms their enantiopurity. Circular Dichroism (CD) and absorption spectroscopies in the NIR reveal sharp $^2F_{7/2} \rightarrow {}^2F_{5/2}$ f–f transitions, with g_{abs} values up to 0.07, indicating a chiral environment for the ytterbium centre. Furthermore, a dynamic mechanism with mixing of ligand states is shown to contribute to the CD intensity. X-band pulse Electron Paramagnetic Resonance spectroscopy, on a magnetically dilute single crystal containing 1% of Yb^{III} complexes within the isostructural Y^{III} diamagnetic host, reveals a phase memory time, T_m, of the electronic spin of 600 ns and that it can be coherently manipulated by microwave pulses, as evidenced by Rabi nutations.

Received 18th April 2025,
Accepted 22nd August 2025

DOI: 10.1039/d5qi00977d

rsc.li/frontiers-inorganic

Introduction

Coherent manipulation of electron spins has been proposed as the foundation of various technological applications within the broad context of Quantum Technologies (QTs).[1,2] QTs encompass technologies that exploit fundamental quantum mechanical properties of matter such as superposition and entanglement to obtain superior performance, previously unattainable by classical counterparts.[3] These new technologies are of interest for a broad range of applications, ranging for example from quantum computers[4] to highly sensitive sensors.[5] Molecules have been proposed as quantum hardware due to several attributes which make them promising qubits or qudits, such as their long coherence times at high temperatures,[6] their tunability and diversity, allowing for a near-infinite number of possibilities for these materials.[7–11] Yb(trensal), is a trigonal lanthanide coordination complex,[12] which was recently shown to possess a suitable electron spin phase memory time, T_m, and the ability to be coherently manipulated, indicating its potential as an electron qubit.[13] Implementation of quantum error correction protocols was demonstrated using the hyperfine coupling of the electronic spin to the ^{173}Yb nucleus[14] and this coupling was later used for the implementation of a quantum simulator on the electronuclear qudit.[15] Furthermore, dipolar coupled Yb^{III} sites could be coherently manipulated, demonstrating quantum gates between two dipolarly coupled entangled qubits.[16]

Coherently addressing and manipulating the state of a spin qubit, such as a molecular spin, is typically achieved by use of magnetic dipole transitions induced by the oscillating magnetic field component of microwave pulses in an externally applied magnetic field.[17] However, a very interesting alternative avenue is the potential substitution of microwave pulses with the application of electric fields coupled to the spin qubit,[18] the magnetic dipole transition in this case being mediated by the magneto-electric coupling.[19] Furthermore, electric fields can be used to tune the resonance frequency of molecular qubits and could be used to selectively bring specific qubits on and off resonance within multiqubit processor setups.[20] The main advantages of using electric rather than magnetic fields include the ability to control electronics on a nanosecond timescale, the highly precise electronics instrumentation already developed and the very power-efficient operation of electronic circuits.[21–23] Efficient coupling of molecular spins to electric fields requires absence of an inversion centre at the molecular level.[20,24] Hence, designing new chiral molecules with relevant properties for quantum information processing or other QTs is of great interest.[25] Since Yb(trensal) has been shown to display numerous properties of interest for QTs, an enantiomeric pure analogue of Yb(trensal) would provide an interesting avenue for studying chiral effects related to quantum information processing. From a preparative per-

[a]*Department of Chemistry, University of Copenhagen, Universitetsparken 5, 2100, Denmark. E-mail: piligkos@chem.ku.dk*
[b]*EaStCHEM School of Chemistry, Biomedical Sciences Research Complex, and Centre of Magnetic Resonance, University of St Andrews, North Haugh, St Andrews KY16 9ST, UK. E-mail: beb2@st-andrews.ac.uk*

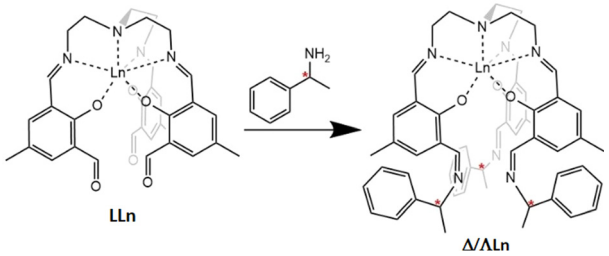

Fig. 1 Reaction scheme for post-functionalisation of **LLn** with methylbenzylamine. Red asterisks indicate the stereogenic centre.

spective, there is only a very limited number of options available for the synthesis of enantiomerically pure lanthanide complexes where chirality is due to the helicity of the coordination sphere environment. This is due to the very small stabilisation effect of the ligand field, resulting in near instantaneous racemization in these complexes in solution.[26] Therefore, the synthesis of chiral lanthanide complexes often involves reacting a simple lanthanide salt or nonchiral coordination complex with a previously synthesized enantiomerically pure ligand,[27–35] or by precipitation of an ionic complex with a chiral counterion.[27] We have previously shown that post-functionalization of the complex **LLn** (Fig. 1), with Ln = Gd, Tb, Dy, Ho, Er, Tm, Yb or Lu, with primary amines provides a direct route towards adding desired properties to Ln-based coordination complexes.[36] In these previous studies we have only used non-chiral amines.[37,38] Herein, we demonstrate that condensation of **LYb** with an enantiomerically pure primary amine (*S*- or *R*-methyl-benzylamine) provides the means to form chiral ytterbium complexes exhibiting coordination sphere helicity (**ΔYb** or **ΛYb**), an avenue that has not been previously explored for trensal-like ligands. These studies affirm the versatility of our post-functionalization approach to synthesize functional coordination compounds. The chiroptical properties of the synthesized ytterbium complexes are examined, and their origin investigated. Furthermore, these chiral materials are examined by a combination of continuous wave (c.w.) and pulse Electron Paramagnetic Resonance (EPR) spectroscopy demonstrating that they retain a suitable phase memory time and the ability of their electronic spin to be coherently manipulated by microwave pulses.

Experimental section

The parent complex, **LYb**, was synthesised according to literature procedures.[36] All reagents were purchased from commercial sources and used as received.

Synthesis of ΔYb/ΛYb

LYb (200 mg, 0.265 mmol) was suspended in a 1 : 1 chloroform/methanol solution (20 ml) and *S*- or *R*-methyl-benzylamine (0.4 ml, 3 mmol) was added resulting in **ΔYb** or **ΛYb**, respectively (*vide infra*). The reaction was stirred for 1 hour after which a clear solution was obtained. 200 ml diethylether were added to the solution which was covered with a glass cover and left to crystalize for 2–4 days.

Yield: around 160 mg, 58%. Compositional and phase purity was confirmed by elemental analysis (Table S1), IR (Fig. S11 and S12), and X-ray powder diffraction (Fig. S15).

^{1}H-NMR (Fig. S16–S18) was obtained using a Bruker 500 MHz instrument equipped with a cryoprobe. For ^{1}H-NMR calibration was done against solvent signals from the deuterated solvent. Positive-ion mode MALDI mass spectrometry (Fig. S19–S22) was performed on a Bruker Solarix XR 7T ESI/MALDI FT-ICR MS instrument at the Department of Chemistry, University of Copenhagen. Elemental (C, H, and N) analyses were performed on a FlashEA 1112 instrument at The Microanalytical Laboratory at the Department of Chemistry, University of Copenhagen.

Single crystals were measured on a BRUKER D8 VENTURE diffractometer equipped with a Mo Kα High-brilliance IμS 53 radiation source (λ = 0.71073 Å). A PHOTON 100 CMOS detector was employed. The instrumentation was controlled using APEX2. The sample was cooled to 120 K using an Oxford cryosystem. The resulting data were modelled using SHELXT with intrinsic phasing and refined using SHELXL (Least squares).[39] Visualisation of the refinement process was done using OLEX2.[40] Hydrogens were added using the "Add H" function in Olex2 and refined isotopically, while all non-hydrogen atoms were refined anisotropically.[40]

Absorption spectroscopy was performed on a PerkinElmer Lambda 2 UV/Vis spectrometer with a 2 nm slit width. Circular dichroism (CD) was measured on a Jasco J1700 equipped with an InGaAs detector for NIR with a 5 nm slit. Both Absorption and CD (Fig. 3, S13 and S14) were measured in approximately 15 mg ml^{-1} solutions in chloroform in 10.0 mm path quartz cuvettes. Absorption and CD were measured back to back on the same cuvette. Infrared spectra were measured on polycrystalline samples on an Agilent Technologies Cary 630 FTIR.

EPR spectra were measured on a magnetically dilute sample of **ΛYb** in the isostructural diamagnetic **ΛY** host lattice at a concentration of 1% ($\mathbf{\Lambda Y_{0.99}Yb_{0.01}}$), as determined by Inductively Coupled Plasma Mass Spectrometry (ICP-MS). X-band c.w.-EPR data were measured on a polycrystalline powder sample using a BRUKER E500 EPR spectrometer fitted with a Bruker X-band ER4122 SHQE cavity resonator. The measurements were performed at 20 K using an Oxford Instruments helium flow cooling system.

Single crystal pulse EPR was measured on a BRUKER X-band E580 EPR spectrometer fitted with an MS3 resonator appropriate for smaller samples and offering higher B_1 excitation fields, on single crystals of approximate size 0.2 × 0.2 × 3 mm.^{3} A cryogen free variable temperature cryostat from Cryogenics Ltd was used. Echo-Detected Field-Swept (EDFS) EPR spectra were measured using a standard Hahn echo sequence ($\pi/2$–τ–π–τ-echo) with $\pi/2$ = 16 ns. T_m was measured by recording the time evolution of the Hahn echo, with $\pi/2$ = 128 ns to decrease ESEEM (electron spin echo envelope modulation). Spin lattice relaxation, T_1, was measured using a stan-

dard inversion recovery sequence (π–T–$\pi/2$–τ–π–τ-echo) with $\pi/2$ = 16 ns. Both T_1 and T_m were modelled as mono-exponential decays. Transient nutation was measured using a θ–T–$\pi/2$–τ–π–τ-echo sequence with θ the nutation pulse angle and T = 5000 ns, at 6 different power levels between 6–18 dB.

The c.w.- and EDFS EPR spectra were fitted using Pepper in Easyspin (version 6).[41] EDFS spectra can be assimilated to zero-th derivative c.w. spectra in cases where T_m is the same for all observed transitions and ESEEM or other dynamic modulation effects affecting individual echo intensities are negligible. The single crystal orientation was determined by fitting the sample orientation and molecular frame using the spin Hamiltonian parameters obtained for the polycrystalline powder.

Results and discussion

Reaction of the previously studied complex, **LLn** with enantiomerically pure *S*- or *R*-methyl-benzylamine *via* a Schiff-base reaction in a mixture of chloroform and methanol results in the formation of **ΔYb** or **ΛYb**, respectively, depending on the chirality of the amine (Fig. 1). The resulting complexes crystalize as planks upon addition of diethyl ether, resulting to single crystals suitable for single crystal X-ray diffraction. Single crystal X-ray diffraction revealed that both enantiomers crystallise in the triclinic Sohncke space group $P2_12_12_1$ (Table S2). The crystal structure (Fig. 2) reveals that the ytterbium ion is heptacoordinated by three phenoxides, three imines and a tertiary amine. A pseudo (non-crystallographic) threefold axis passes through the tertiary amine and the Ln-centre. This pseudo-C_3 axis is very close to being ideal with bond lengths and angles only diverging slightly from trigonal symmetry. The imine (N_{imi}–Ln) and phenoxide (Ln–O) bond lengths vary in the range 2.395(4)–2.429(4) Å and 2.154(4)–2.159(4) Å, respectively. **ΔYb** or **ΛYb** show very comparable bond lengths and angles to **LLn** (Table 1 and Tables S3–S6) indicating only very minor perturbation of the Ln environment, as was also seen in previous post-functionalisation experiments employing **LYb**.[36–38] The three chiral methyl-benzylamine arms have their methyl groups pointing towards the central pseudo-C_3 axis of the molecule while their phenyl groups point outward. The asymmetric unit contains the whole molecule, resulting in four identical molecules in the unit cell (Fig. S1–S8). These four units all share the same helicity around the Ln centre, which is dictated by the chiral amine with the *S*-methyl-benzylamine leading exclusively to a Δ helicity around the lanthanide centre while *R*-methyl-benzylamine leads to a Λ one (Fig. S9 and S10). Hence the solid-state structure exclusively contains one helicity, which has not been observed for any previous Ln(trensal)-like complex where both enantiomers co-crystalize resulting to crystals containing both enantiomers.

Table 1 Comparison of selected average bond lengths and bond angles of **LYb**[36] and the chiral post functionalized complexes **ΔYb/ΛYb**

	N_{api}–Ln/Å	N_{imi}–Ln/Å	O–Ln/Å	(N_{api}–Ln–O)/°
LYb	2.609(3)	2.420(2)	2.160(2)	127
ΔYb/ΛYb	2.597(3)	2.412(2)	2.156(2)	125

Chiral molecules interact differently with left and right circularly polarised light because they break space parity symmetry. **ΔYb** or **ΛYb** display several absorption bands between 900–1050 nm belonging to the $^2F_{7/2} \rightarrow {}^2F_{5/2}$ transition, with the three major bands (marked **a**–**c** in Fig. 3) displaying fine structure which is assigned as vibrational fine structure (Fig. 3). The intensity of these transitions is very weak (ε < 20 L mol^{-1} cm^{-1}) which is characteristic for lanthanides.[42] Two minor absorption bands (marked d_h) are assigned as hot-bands due to their emergence at lower energy and being of very weak intensity, in agreement with previous observations for Yb(tensal).[12] The nearly identical absorption spectra in the solid state and in solution indicate dissolution of complexes without major structural changes or decomposition. This is supported by ^{1}H-NMR (Fig. S16–S18) and MALDI-MS (Fig. S19–S22). The CD spectra of the $^2F_{7/2} \rightarrow {}^2F_{5/2}$ transitions are mirror

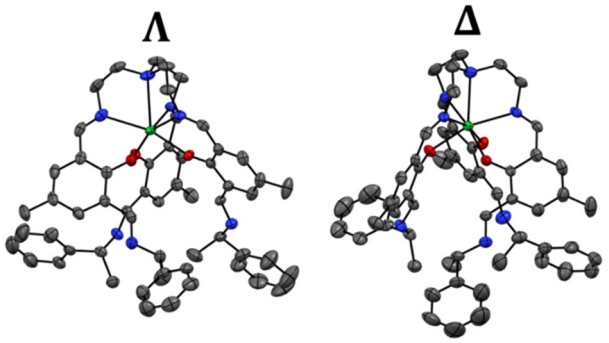

Fig. 2 Crystal structure of **ΔYb** and **ΛYb** seen from the side showing the different handedness of the structures. Colour code: Yb (green), N (Blue), O (red). Hydrogen atoms were omitted for clarity.

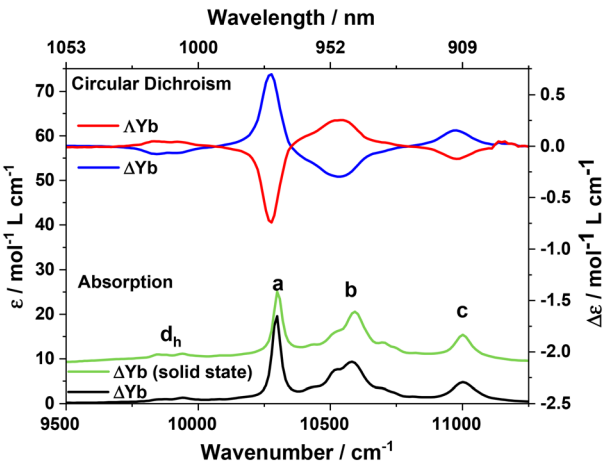

Fig. 3 Absorption and CD spectra of **ΔYb** and **ΛYb** in chloroform. A solid-state absorption spectrum of **ΔYb** is also shown. Labels are defined in the main text.

images of each other with altering phase for various transients. The largest CD signal is observed at transition **a** which shows a $\Delta\varepsilon$ = 0.7 L mol^{-1} cm^{-1} and the largest dissymmetry factor, g_{abs} = 0.07. Although the theoretical maximum absolute value of g_{abs} is 2, typical values for chiral organic molecules or transition metal complexes lie in the range 10^{-4} to 10^{-2}, with lanthanide complexes displaying in general values above this range, sometimes even close to the theoretical maximum.[43–45] Thus, the dissymmetry displayed by **ΔYb** or **ΛYb** is sizeable but not exceptional for f–f transitions. This sizeable dissymmetry indicates that the relevant Yb centre feels a chiral electric potential. Thus, a strong magneto-electric response to electric fields is possible. The origin of the CD signal can either be *via* a static (mixing with ytterbium-based 5d orbitals) or dynamic (mixing with exited states of the ligand) mechanism. For a purely Ln-centred transition to have a transition moment, the transition must contain in part some 5d orbital component to be parity allowed. This is mediated by the dissymmetric ligand allowing this mixing. Due to sum rules the integral of the whole band is hence zero.[46] On the other hand, a dynamic mechanism involves polarisation from the ligand which allows for transitions to be slightly allowed. However, due to mixing with the ligand, the integral of the transition can be non-zero.[46] The integral of the CD spectra of **ΔYb**/**ΛYb** show clear symmetric divergence from zero (Fig. S13), suggesting that some of the intensity of the CD spectra originates from polarisation from the ligand. Hence, designing ligands which facilitate mixing of the lanthanide orbitals with exited states of the ligand could provide a path towards very sensitive electric field coupling.

Having shown that the Yb^{III} centre experiences a chiral environment due to the dissymmetry induced by the chiral ligand, we now examine whether condensation with a chiral amine perturbs its susceptibility to coherent manipulation by microwave pulses, as compared to **LYb**. Detailed information about the *g*- and hyperfine coupling tensor, *A*, of **ΔYb**/**ΛYb** was obtained from c.w.-EPR spectra on polycrystalline **ΛY$_{0.99}$Yb$_{0.01}$** (Fig. 4). The c.w.-EPR spectrum was modelled as originating from an effective S = 1/2 system, due to the large zero field splitting of the eigenstates of the $^2F_{7/2}$ term, resulting in a thermally isolated ground Kramers doublet. The following Hamiltonian was used to model the obtained c.w.-EPR spectra:

$$\hat{H} = \mu_B B_0 g \hat{S} + \hat{S} A \hat{I}$$

The fit (χ^2 = 0.0163) matches the experimental data very well (Fig. 4) and results to the following best-fit parameters: g_x = 2.574(2), g_y = 3.274(0), g_z = 3.697(2), A_x = 523(4) MHz, A_y = 664(2) MHz, A_z = 766(4) MHz.

The resulting parameters are within the range observed for other similar systems based on the Yb(trensal) motive.[12,36,47] In contrast to these other systems, **ΔYb**/**ΛYb** display rhombic *g*- and hyperfine exchange tensors, even though to a good approximation the molecule possesses trigonal symmetry. However, unlike similar molecules, **ΔYb**/**ΛYb** do not possess strict crystallographic trigonal symmetry, hence allowing the *g*- and hyperfine exchange tensors to be rhombic. These observations illustrate the importance of, and the necessity for, strict crystallographic symmetry for obtaining systems characterised by Hamiltonians of accordingly high symmetry.

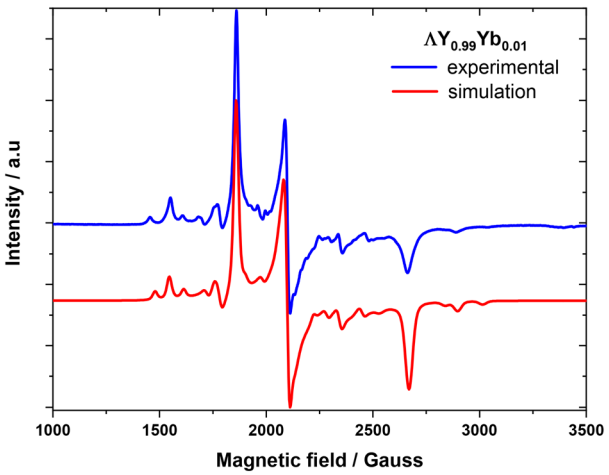

Fig. 4 X-band (9.63 GHz) c.w.-E.P.R. of polycrystalline **ΛY$_{0.99}$Yb$_{0.01}$**, at 20 K.

Pulse-EPR measurements were conducted on a single crystal of **ΛY$_{0.99}$Yb$_{0.01}$** for which orientation selectivity between the four different magnetically inequivalent sites of the unit cell was possible without overlapping contributions, as would be the case for a polycrystalline sample. This also results to long Rabi nutation traces possible due to the larger B_1-field homogeneity over the single crystal, as compared to the one for polycrystalline powder samples which are intrinsically less homogeneous. The specific orientation was chosen such that a large magnetic field splitting between the observed lines was obtained (Fig. 5). The EDFS spectrum reveals 4 major lines,

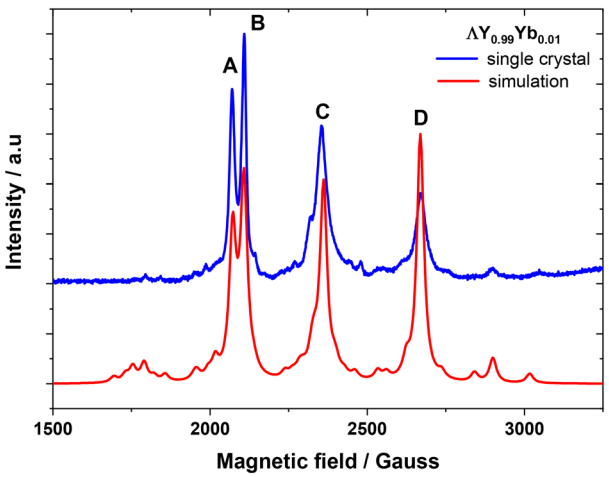

Fig. 5 Single crystal EDFS of **ΛY$_{0.99}$Yb$_{0.01}$** measured at 5 K using a standard Hahn echo sequence, as described in the experimental section. Main transitions are labelled **A**–**D**. Simulation (red) based on best fit from the polycrystalline sample.

labelled **A–D** in Fig. 5, each corresponding to one of the 4 different magnetically inequivalent orientations of crystallographically identical Yb^{III} sites within the crystal possessing no nuclear spin ($I = 0$). The smaller peaks observed originate from hyperfine coupling to the less abundant ^{173}Yb and ^{171}Yb isotopes possessing a nuclear spin, $I = 5/2$ and $I = 1/2$, respectively. The dynamics of the **A–D** lines (Fig. S23–S30 and Tables S7 and S8) originating from $I = 0$ isotopes were measured for all 4 inequivalent orientations within the sample (Fig. 5 and 6). Slightly longer T_m's than for Yb(trensal) were observed at similar doping level (1%), likely due to the methyl-benzyl arms increasing the average distance between paramagnetic centres. T_1 shows a steep temperature dependence, $T_1 \propto T^{-4.4}$, which is also observed for similar ytterbium compounds due to the large orbital angular momentum of the ground state resulting in strong coupling to the lattice. Consequently, T_m slowly decreases with increasing temperatures, with 14 K being the highest temperature at which an echo is detectable, due to T_1 limiting T_m at higher temperatures. This limit is however slightly lower than for Yb(trensal) which is T_1-limited at around 20 K. This difference could originate from the increase of the number of phonons resulting from the introduction of the extra benzyl amine moieties.

Transient nutation experiments display clear oscillations of the echo intensity (Rabi oscillations) with nutation pulse duration (Fig. 7 and S31–S34). As expected, the Rabi frequencies, extracted by Fourier Transform of transient nutation traces (Fig. S35–S38), show a linear dependence to microwave power (B_1). The Rabi frequencies at a given B_1 come in pairs with the **A** and **B** resonances in general showing slower nutation frequencies than the **C** and **D** ones, due to the anisotropic g-tensor. This indicates that the orientation of the sample plays an important role for the Rabi frequency, for systems with large g-tensor anisotropy. Transitions **A–D** display more than 30 coherent oscillations indicative of a homogenous B_1 field across the sample. Observation of a large number of Rabi oscillations is indicative of potential for high fidelity of operations to be implemented on the system.

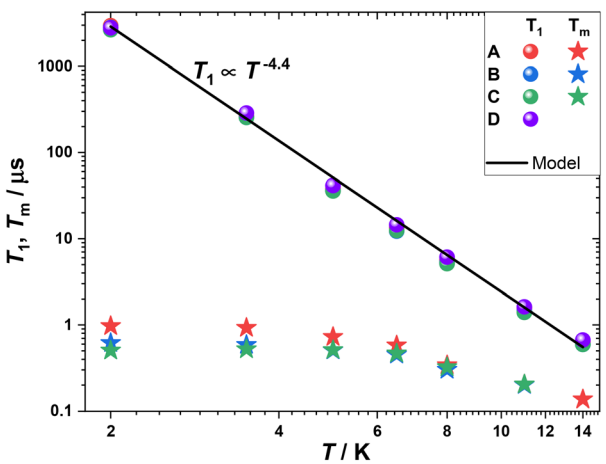

Fig. 6 Temperature dependence of T_1 and T_m for the four main transitions **A–D** of $\Lambda Y_{0.99}Yb_{0.01}$. A model of $T_1 \propto T^{-4.4}$ is shown as a black line.

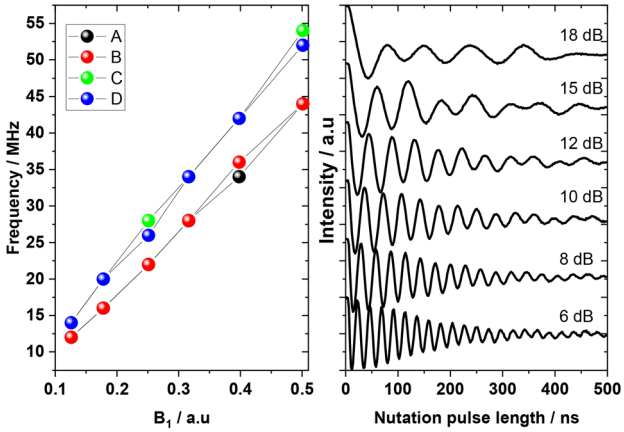

Fig. 7 Left: Rabi frequencies for the four transitions **A–D** of $\Lambda Y_{0.99}Yb_{0.01}$ *versus* B_1. Right: Rabi nutation at various power levels for transition **A**.

Conclusion

We show herein that post functionalization of an aldehyde containing lanthanide complex (**LYb**) with chiral primary amines provides a route to chiral lanthanide complexes. Circular dichroism and absorption spectroscopy studies of the obtained chiral complexes evidenced clear f–f transitions for Yb characterised by large g_{abs} values of the order of 0.07 for which a dynamic mechanism involving the ligand contributes to the CD intensity. This provides a potential design criterion for the development of molecular materials exhibiting strong magnetoelectric coupling. Furthermore, we show that under the conditions of this study **ΔYb**/**ΛYb** display a phase memory time of about 0.5 to 1 μs and that the electronic spin can be coherently manipulated by microwave pulses. The frequency of the observed Rabi oscillations is orientation dependent for these systems characterised by strongly anisotropic g-factor. Hence, we create herein an Yb(trensal) analogue showing chiroptical properties while retaining similar coherent dynamic properties as the parent **LYb**. These results establish the family of Yb (trensal) complexes and derivatives as an avenue for further studies of chirality induced effects on the coherent dynamics of molecular materials relevant for quantum technologies. The complexes discussed herein being enantiopure, offer the advantage that they might give access to studies that might not be feasible in crystals of chiral molecular complexes containing both enantiomers, as is the case for example for Yb(trensal).

Author contributions

The project was jointly conceived by CDB, SHH and SP. CDB and SHH prepared the samples. BEB and SHH performed the

measurements. SHH performed the data analysis, supervised by SP and BEB. The manuscript was written jointly by all authors, who all have read and agreed to the final version of the manuscript.

Conflicts of interest

There are no conflicts to declare.

Data availability

The research data supporting this publication will be freely accessible at **https://doi.org/10.17630/443f0aa3-c7a6-4b8c-9abe-874d88c5b6f3**.

Supplementary information is available. See DOI: **https://doi.org/10.1039/d5qi00977d**.

CCDC 2428735 (**ΔYb**), 2428867 (**ΛYb**), 2428550 (**ΔY**) and 2428518 (**ΛY**) contains the supplementary crystallographic data for this paper.[48a–d]

All structures were measured at 120 K.

Acknowledgements

We thank the Novo Nordisk Foundation for research grants NNF20OC0065610 Project Grants in the Natural and Technical Sciences 2020, NNF21OC0068806 Research Infrastructure – Large equipment and facilities 2021 financing the Copenhagen Pulse-EPR Facility, NNF21OC0070832 Exploratory Inter-disciplinary Synergy Programme 2021 and NNF23OC0083201 NERD – New Exploratory Research and Discovery 2023. BEB thanks BBSRC (BB/R013780/1) for funding.

References

1 M. Atzori and R. Sessoli, The Second Quantum Revolution: Role and Challenges of Molecular Chemistry, *J. Am. Chem. Soc.*, 2019, **141**, 11339–11352.
2 M. F. Riedel, I. Bloch, T. Debuisschert, F. Wilhelm-Mauch, V. Pruneri, N. V. Vitanov, S. Wehner and T. Calarco, Europe's Quantum Flagship is taking off, *Europhys. News*, 2018, **49**, 30–34.
3 A. G. J. MacFarlane, J. P. Dowling and G. J. Milburn, Quantum technology: the second quantum revolution, *Philos. Trans. R. Soc. London, Ser. A*, 2003, **361**, 1655–1674.
4 A. Ekert and R. Jozsa, Quantum computation and Shor's factoring algorithm, *Rev. Mod. Phys.*, 1996, **68**, 733–753.
5 G. Czap, P. J. Wagner, F. Xue, L. Gu, J. Li, J. Yao, R. Wu and W. Ho, Probing and imaging spin interactions with a magnetic single-molecule sensor, *Science*, 2019, **364**, 670–673.
6 A. Ardavan, O. Rival, J. J. L. Morton, S. J. Blundell, A. M. Tyryshkin, G. A. Timco and R. E. P. Winpenny, Will Spin-Relaxation Times in Molecular Magnets Permit Quantum Information Processing?, *Phys. Rev. Lett.*, 2007, **98**, 057201.
7 M. R. Wasielewski, M. D. E. Forbes, N. L. Frank, K. Kowalski, G. D. Scholes, J. Yuen-Zhou, M. A. Baldo, D. E. Freedman, R. H. Goldsmith, T. Goodson, M. L. Kirk, J. K. McCusker, J. P. Ogilvie, D. A. Shultz, S. Stoll and K. B. Whaley, Exploiting chemistry and molecular systems for quantum information science, *Nat. Rev. Chem.*, 2020, **4**, 490–504.
8 A. Gaita-Ariño, F. Luis, S. Hill and E. Coronado, Molecular spins for quantum computation, *Nat. Chem.*, 2019, **11**, 301–309.
9 E. Coronado, Molecular magnetism: from chemical design to spin control in molecules, materials and devices, *Nat. Rev. Mater.*, 2020, **5**, 87–104.
10 A. Chiesa, A. Privitera, E. Macaluso, M. Mannini, R. Bittl, R. Naaman, M. R. Wasielewski, R. Sessoli and S. Carretta, Chirality-Induced Spin Selectivity: An Enabling Technology for Quantum Applications, *Adv. Mater.*, 2023, **35**, 2300472.
11 C. Train, M. Gruselle and M. Verdaguer, The fruitful introduction of chirality and control of absolute configurations in molecular magnets, *Chem. Soc. Rev.*, 2011, **40**, 3297–3312.
12 K. S. Pedersen, J. Dreiser, H. Weihe, R. Sibille, H. V. Johannesen, M. A. Sørensen, B. E. Nielsen, M. Sigrist, H. Mutka, S. Rols, J. Bendix and S. Piligkos, Design of Single-Molecule Magnets: Insufficiency of the Anisotropy Barrier as the Sole Criterion, *Inorg. Chem.*, 2015, **54**, 7600–7606.
13 K. S. Pedersen, A.-M. Ariciu, S. McAdams, H. Weihe, J. Bendix, F. Tuna and S. Piligkos, Toward Molecular 4f Single-Ion Magnet Qubits, *J. Am. Chem. Soc.*, 2016, **138**, 5801–5804.
14 R. Hussain, G. Allodi, A. Chiesa, E. Garlatti, D. Mitcov, A. Konstantatos, K. S. Pedersen, R. De Renzi, S. Piligkos and S. Carretta, Coherent Manipulation of a Molecular Ln-Based Nuclear Qudit Coupled to an Electron Qubit, *J. Am. Chem. Soc.*, 2018, **140**, 9814–9818.
15 S. Chicco, G. Allodi, A. Chiesa, E. Garlatti, C. D. Buch, P. Santini, R. De Renzi, S. Piligkos and S. Carretta, Proof-of-Concept Quantum Simulator Based on Molecular Spin Qudits, *J. Am. Chem. Soc.*, 2024, **146**, 1053–1061.
16 B. E. Bode, E. Fusco, R. Nixon, C. D. Buch, H. Weihe and S. Piligkos, Dipolar-Coupled Entangled Molecular 4f Qubits, *J. Am. Chem. Soc.*, 2023, **145**, 2877–2883.
17 G. Aromí, F. Luis and O. Roubeau, in *Lanthanides and Actinides in Molecular Magnetism*, 2015, pp. 185–222, DOI: **10.1002/9783527673476.ch7**.
18 K. C. Nowack, F. H. L. Koppens, Y. V. Nazarov and L. M. K. Vandersypen, Coherent Control of a Single Electron Spin with Electric Fields, *Science*, 2007, **318**, 1430–1433.
19 Z. Liu, Y. X. Wang, Y. H. Fang, S. X. Qin, Z. M. Wang, S. D. Jiang and S. Gao, Electric field manipulation enhanced by strong spin-orbit coupling: promoting rare-earth ions as qubits, *Natl. Sci. Rev.*, 2020, **7**, 1557–1563.

20 J. Liu, J. Mrozek, A. Ullah, Y. Duan, J. J. Baldoví, E. Coronado, A. Gaita-Ariño and A. Ardavan, Quantum coherent spin–electric control in a molecular nanomagnet at clock transitions, *Nat. Phys.*, 2021, **17**, 1205–1209.
21 M. Trif, F. Troiani, D. Stepanenko and D. Loss, Spin-Electric Coupling in Molecular Magnets, *Phys. Rev. Lett.*, 2008, **101**, 217201.
22 A. Laucht, J. T. Muhonen, F. A. Mohiyaddin, R. Kalra, J. P. Dehollain, S. Freer, F. E. Hudson, M. Veldhorst, R. Rahman, G. Klimeck, K. M. Itoh, D. N. Jamieson, J. C. McCallum, A. S. Dzurak and A. Morello, Electrically controlling single-spin qubits in a continuous microwave field, *Sci. Adv.*, 2015, **1**, e1500022.
23 S. Asaad, V. Mourik, B. Joecker, M. A. I. Johnson, A. D. Baczewski, H. R. Firgau, M. T. Mądzik, V. Schmitt, J. J. Pla, F. E. Hudson, K. M. Itoh, J. C. McCallum, A. S. Dzurak, A. Laucht and A. Morello, Coherent electrical control of a single high-spin nucleus in silicon, *Nature*, 2020, **579**, 205–209.
24 M. Fittipaldi, A. Cini, G. Annino, A. Vindigni, A. Caneschi and R. Sessoli, Electric field modulation of magnetic exchange in molecular helices, *Nat. Mater.*, 2019, **18**, 329–334.
25 C. D. Aiello, *et al.*, A Chirality-Based Quantum Leap, *ACS Nano*, 2022, **16**, 4989–5035.
26 H.-Y. Wong, W.-S. Lo, K.-H. Yim and G.-L. Law, Chirality and Chiroptics of Lanthanide Molecular and Supramolecular Assemblies, *Chem*, 2019, **5**, 3058–3095.
27 H. C. Aspinall, Chiral Lanthanide Complexes: Coordination Chemistry and Applications, *Chem. Rev.*, 2002, **102**, 1807–1850.
28 G. Handzlik, K. Rzepka and D. Pinkowicz, The Underexplored Field of Lanthanide Complexes with Helicene Ligands: Towards Chiral Lanthanide Single Molecule Magnets, *Magnetochemistry*, 2021, **7**, 138.
29 J. W. Walton, R. Carr, N. H. Evans, A. M. Funk, A. M. Kenwright, D. Parker, D. S. Yufit, M. Botta, S. De Pinto and K.-L. Wong, Isostructural Series of Nine-Coordinate Chiral Lanthanide Complexes Based on Triazacyclononane, *Inorg. Chem.*, 2012, **51**, 8042–8056.
30 M. Gucma, W. M. Gołębiewski, E. Romanowska and W. Skupiński, Application of Different Spectral Methods to Examine Structure of the Complexes Found in the Cycloaddition Reactions of 4-Trifluoromethylbenzonitrile Oxide to Olefins, *Appl. Magn. Reson.*, 2013, **44**, 1359–1371.
31 K. Kumar, O. Stefanczyk, K. Nakabayashi, K. Imoto, Y. Oki and S.-i. Ohkoshi, Detection of Sub-Terahertz Raman Response and Nonlinear Optical Effects for Luminescent Yb(III) Complexes, *Adv. Opt. Mater.*, 2022, **10**, 2101721.
32 X. Du, Z. Zhang, C. Gao, F. Li and X.-L. Li, Two pairs of chiral YbIII enantiomers presenting distinct NIR luminescence and circularly polarized luminescence performances with giant differences in second-harmonic generation responses, *Dalton Trans.*, 2023, **52**, 17758–17766.
33 X.-L. Li, A. Wang, Y. Li, C. Gao, M. Cui, H.-P. Xiao and L. Zhou, Two Chiral YbIII Enantiomeric Pairs with Distinct Enantiomerically Pure N-Donor Ligands Presenting Significant Differences in Photoluminescence, Circularly Polarized Luminescence, and Second-Harmonic Generation, *Inorg. Chem.*, 2023, **62**, 4351–4360.
34 A. Sickinger, M. Grasser, B. Baguenard, A. Bensalah-Ledoux, L. Guy, A. T. Bui, Y. Guyot, V. Dorcet, F. Pointillart, O. Cador, S. Guy, O. Maury, B. Le Guennic and F. Riobé, Temperature-dependent NIR-CPL spectra of chiral Yb(iii) complexes, *Phys. Chem. Chem. Phys.*, 2024, **26**, 15776–15783.
35 I. Shioukhi, L. C. Adi, V. Dorcet, O. Cador, G. L. J. A. Rikken, B. Le Guennic, J. Crassous, C. Train, F. Pointillart, M. Atzori and O. Gidron, Magneto-chiral dichroism in a chiral twistacene ytterbium(iii) one-dimensional assembly of single-molecule magnets, *Inorg. Chem. Front.*, 2025, DOI: **10.1039/D5QI00832H**.
36 C. D. Buch, S. H. Hansen, C. M. Tram, D. Mitcov and S. Piligkos, Functionalized Trigonal Lanthanide Complexes: A New Family of 4f Single-Ion Magnets, *Inorg. Chem.*, 2020, **59**, 16328–16340.
37 Y. Zhou, C. D. Buch, S. H. Hansen and S. Piligkos, Long aliphatic chain derivatives of trigonal lanthanide complexes, *Dalton Trans.*, 2023, **52**, 8792–8799.
38 Y. Zhou, C. D. Buch, S. H. Hansen and S. Piligkos, Derivatives of trigonal lanthanide complexes by reaction with long aliphatic chain amines, *C. R. Chim.*, 2024, DOI: **10.5802/crchim.282**.
39 G. M. Sheldrick, Crystal structure refinement with SHELXL, *Acta Crystallogr., Sect. C:Struct. Chem.*, 2015, **71**, 3–8.
40 O. V. Dolomanov, L. J. Bourhis, R. J. Gildea, J. A. K. Howard and H. Puschmann, OLEX2: a complete structure solution, refinement and analysis program, *J. Appl. Crystallogr.*, 2009, **42**, 339–341.
41 S. Stoll and A. Schweiger, EasySpin, a comprehensive software package for spectral simulation and analysis in EPR, *J. Magn. Reson.*, 2006, **178**, 42–55.
42 J.-C. G. Bünzli, S. V. Eliseeva, P. Hänninen and H. Härmä, in *Lanthanide Luminescence: Photophysical, Analytical and Biological Aspects*, Springer Berlin Heidelberg, Berlin, Heidelberg, 2011, pp. 1–45, DOI: **10.1007/4243_2010_3**.
43 G. Albano, G. Pescitelli and L. Di Bari, Chiroptical Properties in Thin Films of π-Conjugated Systems, *Chem. Rev.*, 2020, **120**, 10145–10243.
44 O. G. Willis, F. Zinna, G. Pescitelli, C. Micheletti and L. Di Bari, Remarkable near-infrared chiroptical properties of chiral Yb, Tm and Er complexes, *Dalton Trans.*, 2022, **51**, 518–523.
45 F. S. Richardson, Selection rules for lanthanide optical activity, *Inorg. Chem.*, 1980, **19**, 2806–2812.
46 L. D. Bari and P. Salvadori, in *Comprehensive Chiroptical Spectroscopy*, 2011, pp. 221–246, DOI: **10.1002/9781118120187.ch9**.
47 S. H. Hansen, C. D. Buch and S. Piligkos, Structural isomerism-tuned magnetisation relaxation dynamics in lanthanide coordination complexes, *Inorg. Chem. Front.*, 2024, **11**, 2116–2127.

48 (*a*) S. H. Hansen, C. D. Buch, B. E. Bode and S. Piligkos, CCDC 2428735: Experimental Crystal Structure Determination, 2025, DOI: **10.5517/ccdc.csd.cc2mj99s**; (*b*) S. H. Hansen, C. D. Buch, B. E. Bode and S. Piligkos, CCDC 2428867: Experimental Crystal Structure Determination, 2025, DOI: **10.5517/ccdc.csd.cc2mjfk5**; (*c*) S. H. Hansen, C. D. Buch, B. E. Bode and S. Piligkos, CCDC 2428550: Experimental Crystal Structure Determination, 2025, DOI: **10.5517/ccdc.csd.cc2mj3bm**; (*d*) S. H. Hansen, C. D. Buch, B. E. Bode and S. Piligkos, CCDC 2428518: Experimental Crystal Structure Determination, 2025, DOI: **10.5517/ccdc.csd.cc2mj29k**.